Available online at www.sciencedirect.com

ScienceDirect

Procedia Manufacturing 11 (2017) 1651 – 1658

Procedia MANUFACTURING

27th International Conference on Flexible Automation and Intelligent Manufacturing, FAIM2017, 27-30 June 2017, Modena, Italy

Comparison of commonly used sail cloths through photogrammetric acquisitions, experimental tests and numerical aerodynamic simulations

Michele Calì[a]* , Salvatore Massimo Oliveri[a], Antonio Gloria[b], Massimo Martorelli[c], Domenico Speranza[d]

[a]*Electric, Electronics and Computer Engineering Department, University of Catania, V.le A. Doria, 6 - 95125 Catania (Italy).*
[b]*Institute of Polymers, Composites and Biomaterials , National Research Council of Italy, V.le J.F. Kennedy 54 – Mostra d'Oltremare PAD.20, 80125 Naples – Italy.*
[c]*Department of Industrial Engineering, University of Napoli Federico II, P.le Tecchio, 80 - 80125 Napoli – Italy*
[d]*Department of Civil and Mechanical Engineering, University of Cassino and Southern Lazio, Via G. Di Biasio, 43 - 03043 Cassino (Fr) - Italy*

Abstract

The use of polymer composites has been increasing over the years and nowadays the requirements for designing high performance and lightweight fabrics and laminates for sail manufacturing have become more stringent than ever. The present paper offers an effective methodology that enhances the understanding of the influence of fibres orientation and arrangement of panels on sail performance. Constitutive characteristics of the ten commonly used sail cloths are experimentally measured and their influence on sail dynamic performance is compared using an aerodynamic approach. As expected also in industry 4.0 the method allows to control the production process and final product optimization.

Peer-review under responsibility of the scientific committee of the 27th International Conference on Flexible Automation and Intelligent Manufacturing

Keywords: RE, Digital photogrammetry, CFD analysis, Turbulence model, Aerodynamic coefficient, Apparent wind angle (AWA), Apparent Wind Speed (AWS).

* Corresponding author.
E-mail address: mcali@dii.unict.it

Peer-review under responsibility of the scientific committee of the 27th International Conference on Flexible Automation and Intelligent Manufacturing
doi:10.1016/j.promfg.2017.07.287

1. Introduction

Sail manufacture has undergone significant development due to their implementation and increased application in such sailing races as America's Cup and the Volvo Around-The-World Race. These competitions require advanced technologies to improve sail performance [1, 4]. Interaction between fluid and structure requires a solution which can combine both aerodynamic and structural numerical simulations. The constitutive characteristics (elasticity and structural damping) of materials must be applied accurately in numerical simulations as they have profound impact on the dynamic performance of the sail. Precise elastic orthotropic characteristics must be obtained only by experimental testing. Without recourse to particularly complex mathematical formulations with multilayer elements and significant computational resources, the anisotropic material behaviour and their structural damping values (experimentally measured values) have been introduced in Detached Eddy Simulations (DES) via Shell 181 elements using commercial code ANSYS® (vers 17.0). In this way aeroelastic and turbulent effect on the anisotropic material behaviour for ten nowadays most commonly used sail fabrics was studied and the findings were compared. The use of DES, following the procedure described in Viola et al. [5, 6], enabled a detailed study of the turbulent effects manifested in the interaction between sail and air, highlighting significant differences in behaviour of different sail cloths.

The case study of a symmetric tri-radial Spinnaker of an Elan 31 cruiser-racer, studied by the authors in previous works [7, 8] offers tangible results to support the methodology by validating it with experimental data. Digital photogrammetry was used to get the 3D CAD model of the sail and to validate CAA obtaining the 3D reconstructions of the flying shape for Nylon sail in correspondence with Apparent Wind Speed (*AWS*) of 7.0 knots and *AWA* 185°. This passive techniques allow, through simple and low-cost hardware and software, to get fast and accurate 3D sail acquisitions. Among passive techniques [9, 12], in fact, the digital photogrammetry has known an important development during the last decade due mainly to the increase of the quality of low-cost digital cameras and the significant development of photogrammetric software [13, 15]. The paper is divided into 4 sections, excluding introduction. The first section is devoted to the experimental characterization of the most common sail cloths. The second section deals with sail CAA and its validation with digital photogrammetry. In Section 3 the performance of the ten sail cloths in terms of aerodynamic coefficient (c_p) and *Eddy Turbulence Kinetic Energy* are compared and the main research results are discussed. Final considerations and conclusions are drawn in Sections 4.

Nomenclature

AWA	Apparent Wind Angle [°]
AWS	Apparent Wind Speed [m/s]
Bias	Diagonal across a piece of fabric at 45-degees to the weft and warp
c_p	Aerodynamic coefficient [-]
C_{eq}	Equivalent viscous damping coefficient [-]
Dacron	DuPont's trade name for polyester fibre
DIAX	Bainbridge's brand laminates with a 45-degree diagonal scrim
Kevlar	DuPont's trade name for a family of high-strength aramid fibres
L_t	Tab length [mm]
$\square_{cloth}$	Ccloth density [g/ cm^3]
SS	Specific Strength [MPa×cm^3/g]
σ_u	Ultimate material tensile strength [MPa]
t_{eq}	Equivalent thickness [mm]
t_{mea}	Measured thickness [mm]

2. Sail cloths characterization

All in all, ten sail cloths were characterized by means of replicable experimental and analytical analyses to determine the constitutive behaviour and the *SS* to use in CAA. Sail cloths were supplied by *Velerie Bainbridge*, *Dimension-Polyant GmbH* and *Banks Sails Membrane*. Table 1 shows the main properties and characteristics of the

selected cloths. The fourth column shows the weight in grams of a square meter of cloth. The fifth and sixth columns (in brackets) report the matrix density and the cloth composite density ρ_{cloth}, respectively. However, the seventh and eighth columns report the measured thickness (t_{mea}) and the equivalent thickness (t_{eq}), respectively. In fact, to perform an accurate stress experimental characterization it is important to determine the real cloth density and the corresponding equivalent thickness. These two parameters are related by the following equation: $t_{eq} = \frac{W_{cloth}}{A_s \, \rho_{cloth}}$, where W_{cloth} is the weight of the fabric and A its area.

Conforming to UNI EN ISO 13934-1, 2000 experimental cloth characterization was performed using a ZwickRoell Z100 twin column tensile testing machine (Fig. 1a). and TestXpert® v11.02 software. Tensile tests in warp, weft and bias directions were performed on ten different sail cloths (Fig. 2). Subsequently, the stress-strain curves and the moduli of elasticity were evaluated.

Table 1. Characteristics of sail cloths.

Sample N°	*Cloth*	*Sail Supplier*	*Specific weight* [g/m^2] ([g/cm^3])	*Thickness* [mm] t_{mea} – t_{eq}	*Symmetry*
1	Custom Carbon	Membrane	292.0 (1.38–***1.17***)	0.35– ***0.25***	Long. and Trans
2	Nylon	Polyant	61.8 (1.14–***0.91***)	0.08– ***0.07***	Long. and Trans
3	Kevlar FLEX	Polyant	240.1 (1.29–***1.20***)	0.32– ***0.20***	*none*
4	Hydra Net®	Polyant	396.5 (1.30–***1.22***)	0.43– ***0.33***	Long. and Trans
5	DIAX 60P	Bainbridge	157.1 (1.18–***1.08***)	0.25– ***0.15***	Long. and Trans
6	Kevlar CZ 15	Polyant	97.8 (1.16–***1.04***)	0.18– ***0.09***	Long. and Trans
7	Pentex FLEX 13	Polyant	233.1 (1.18–***1.08***)	0.30– ***0.22***	*none*
8	PX 15T	Polyant	240.6 (1.25–***1.20***)	0.24– ***0.20***	Long. and Trans
9	Pentex FLEX 15	Polyant	226.3 (1.22–***1.13***)	0.26– ***0.20***	Long. and Trans
10	Dacron© TNF 240	Polyant	249.8 (1.37–***1.06***)	0.31– ***0.24***	Long. and Trans

Fig. 1. Zwick & Roell Z100 tensile testing machine.

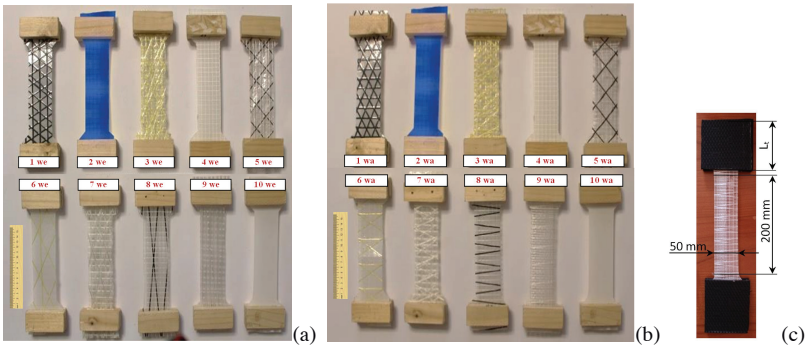

(a) (b) (c)

Fig. 2. Sail cloth samples: (a) in weft direction; (b) in warp direction; (c) specimen dimensions.

2.1. Constitutive characteristics of sail cloths

Each curve which interpolates the tests carried out on five samples is obtained by discretizing within the same number of sampling points (2200) the tests carried out and calculating, at each nominal strain value, the mean value. Fig. 3 shows the results from tensile tests performed in the weft and in the warp direction for the ten sail cloths.

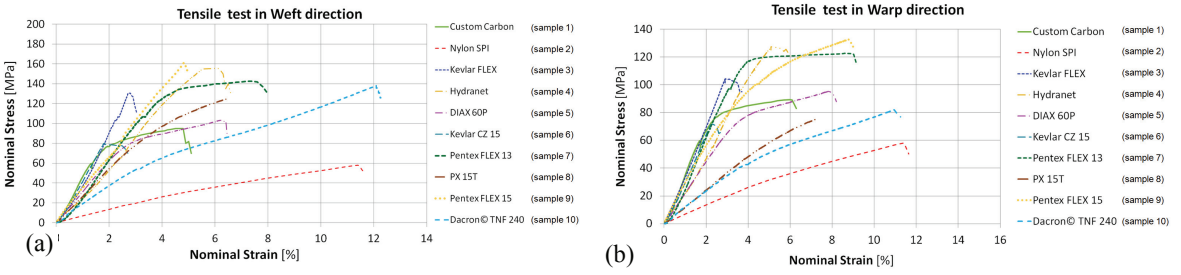

(a) (b)

Fig. 3. Nominal Stress-Nominal Strain curves in: (a) weft direction; (b) warp direction.

Carbon fibres (sample 1), HydraNet (sample 4), polyester (samples 5), Kevlar CZ 15 (sample 6), Pentex FLEX (sample 7 and 9) and PX 15T (sample 8) provided similar stress-strain curves consisting of three different zones: an initial linear elastic region, followed by the second elastic/plastic region with a downward concavity and the third zone after which the cloth yielded. In this region of the curve the cloth continues to provide some resistance (even 40% stretching for some cloths) which decreases with increasing tensile stress.
The modulus of the cloths was evaluated as the slope of the initial linear region. All the samples show initially comparable elastic deformation. The final deformation is on average 200% higher than the elastic one, whereas a reinforced cloth (sample 1, 2, 4, 5, 7, 8 and 9) has much greater plastic deformation tolerance. In all the cases examined, cloth fracture was ductile and occurred after much plastic deformation. Final nominal stress value was quite variable: nominal stress value for HydraNet (sample 4) was about 50% higher than other cloths.

For many cloths the tensile curves in the warp direction are noticeably different to that in the weft direction confirming their marked orthotropy. At low stress level, samples 2, 4, and 10 showed high flexibility (i.e., high strain value), thus indicating lower values of Young's modulus in comparison to the other cloths (Table 2). The specific resistance and the maximum strain for the ten sail cloths are reported in columns 3 and 4 of Table 2.

Table 2. Specific resistance, strain max, strength max, Young's Moduli.

Sample N°	*Cloth*	*SS*	*Strain max* [%]	*Strength max* [MPa]	E_{weft} [MPa]	E_{warp} [MPa]
1	Custom Carbon	80	5.0	95	4100	3700
2	Nylon SPI	94	11.5	59	580	540
3	Kevlar FLEX	113	2.7	132	4200	3800
4	Hydranet	128	5.8	154	2800	2500
5	DIAX 60P	86	6.4	104	2700	2600
6	Kevlar CZ 15	78	2.3	79	2800	2600
7	Pentex FLEX 13	141	7.8	143	3700	3500
8	PX 15T	113	6.3	126	1300	1100
9	Pentex FLEX 15	132	4.7	162	3560	3400
10	Dacron© TNF 240	158	12.2	140	1050	660

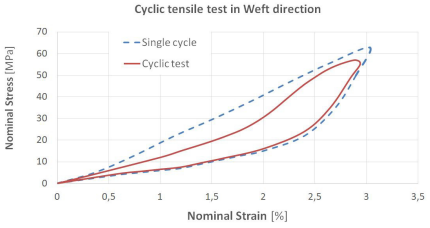

Fig. 4. Dacron© TNF 240 cyclic tensile test in weft direction.

Sample 6, 8 and 10 presented most high values of specific resistance. The energy (E_d) dissipated per unit of volume was evaluated taking into account the loading-unloading cycles (i.e. hysteresis loops) at various frequencies in the linear elastic region of the tensile curves (Fig. 4). The energy dissipated per unit of volume allowed assessing the equivalent viscous damping coefficients [16] as reported below:

$$C_{eq} = \frac{E_d}{2\pi^2 \cdot f \cdot \Delta l_{max}^2} \quad (1)$$

Corresponding to 1 Hz frequency and Δl_{max} values in linear elastic zone during a tensile test in weft direction the equivalent viscous damping coefficients C_{eq} were evaluated according to the equation (1).

Table 3. Equivalent viscous damping coefficient.

Sample N°	*Cloth*	Δl_{max}	E_d	C_{eq}
1	Custom Carbon	1.2	2	0.07
2	Nylon	1.5	1.3	0.03
3	Kevlar FLEX	1.05	1.7	0.08
4	Hydranet	1.7	4	0.07
5	DIAX 60P	2.6	5.3	0.04
6	Kevlar CZ 15	1.3	1	0.03
7	Pentex FLEX 13	2.2	3.8	0.04
8	PX 15T	1.8	3.2	0.05
9	Pentex FLEX 15	2.3	4.2	0.04
10	Dacron© TNF 240	2.8	9.3	0.06

3. Aerodynamic numerical simulations

With the aim of evaluating the influence the calculated sail constitutive relations have on the sail aerodynamic performance, CAA were performed on a tri-radial symmetric spinnaker in a virtual wind tunnel test with with ANSYS® software (vers 17.0). The spinnaker is an integral part of Elan 31, a 9 m long cruiser-racer, produced by the sail-maker Banks Sails Naples with a surface area of 60 m^2 (Fig. 5). Two sheets (length of about 6 m) connect sail's clews to the boat; the boat's halyard is fixed to the head of the main mast. The complex interaction between the fluid and the structure, as well as the continuous change of sail flying shapes make direct numerical simulations unfeasible and therefore aerodynamics turbulence and structural simulations must be modelled jointly. The boundary layer and the wake was modelled with Large Eddy Simulations.

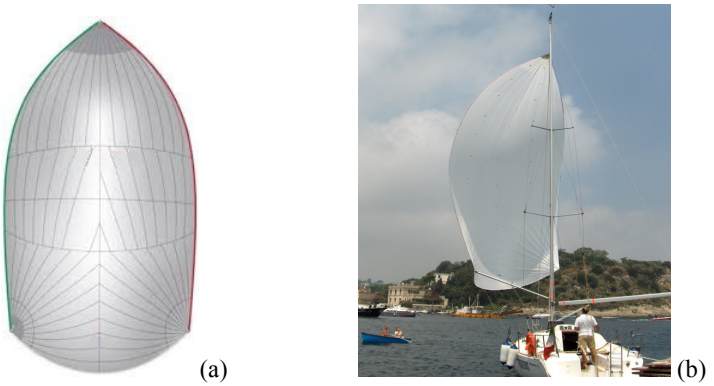
(a) (b)

Fig. 5. (a) Spinnaker designed shape and its arrangement of panels; (b) flying shapes.

3.1. Computational domain and boundary conditions

The sails and sheets were modelled in a non-slip condition. A prismatic computational domain, which was 26 m high, 26 m wide and 65 m long, was used to model a wind tunnel. The non-slip condition was used on the floor boundary which extended 7.2 m downstream from the model. The wind tunnel side-walls and roof were modelled with slip-conditions but the computational domain extended further downstream (minimum 60 m from the sail) than the end of the physical roof and floor, therefore pressure outlet conditions were used for these boundaries.

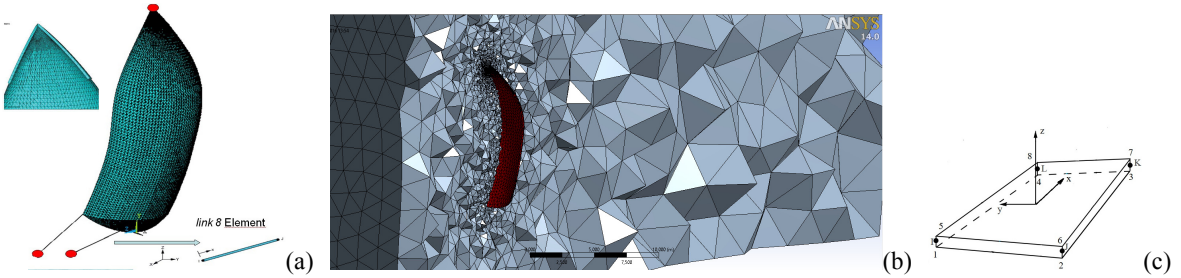

(a) (b) (c)

Fig. 6. (a) sail mesh; (b) air mesh; (c) four node structural shell.

The sail and the sheets were modelled with 1200 shell 181 four-node quadrangular elements in a structured mesh (Fig.6a and 6c). Discretizing enabled the insertion of the linear effects of Young's Moduli in weft and warp directions and the equivalent damping coefficient C_{eq} shown in Tab. 2 and Tab. 3 in CAA. The mesh was refined with pinch control commands and face sizing commands until the growth rate was 1.2 and the skewness was less than 0.95 checking that the maximum dimensions of the elements are not exceeded in simulations, and the linear elastic deformation corresponds to Δl_{max} . Eelements with greater thickness were used to taking into account the

reinforcements applied at the head and clews (Fig. 6a). The air in the wind tunnel was modelled with 489844 tetrahedral elements and 81838 nodes in a non-structured mesh (Fig. 6b).

3.2. Digital photogrammetry acquisition

The limited dimensions of the vessel have made it possible to moor the vessel to the dock making it possible photogrammetry acqusition. With the vessel in a fixed position during the study, the need to evaluate AWS and real wind was avoided. In this conditions also the AWA is the same for a real incident wind angle. From the on-board instrumentation it was possible to detect wind intensity (7.0 knots) and direction (185°).

In order to obtain a points cloud of the sail, which can be used in the validation of the sail model, markers have been placed on the surface of the sail. References to size and color visible from the distance, within which the work was to be carried out, have been distributed over the entire surface, but more densely along the leech, luff, the foot and in the areas of greater curvature (Fig. 7a). Markers were placed on the structures that would remain non-deformed during the study. In particular, on the boom and mast, the purpose of these markers is to acquire two points at a known distance to calculate the scale factor by which to trace back to the actual size of the sail. Photos were acquired using 3 digital cameras cameras (Go Pro Hero 3 Black with a resolution of 12 Mpixels). A camera was placed on the wharf so that the sail could be photographed entirely from the stern. Two others were placed on two small vessels on either side of the sail in order to completely include the luff or leech and half of the foot. This way the three photographs have more points in common making it possible to position them in a photogrammetric scene. The three cameras shot the photos simultaneously to capture the same deformed image of the spinnaker. To return the points cloud of on the surface of the sail photogrammetric software, Photo Modeler Pro from Eos Systems was used. Assuming that all three cameras are identical, only one was calibrated according to typical software procedure. Once the photos have been chosen and acquired homologous points are located and processed in order to obtain a points cloud in the space. From the points detected, interpolating curves have been constructed and then NURBS surfaces inserted (Fig. 7c). The final mesh has been optimized (border regularization) and repaired using the automatic fixing tool as described in [17]. Rhinoceros® 3D (McNeel, Seattle, WA, USA)

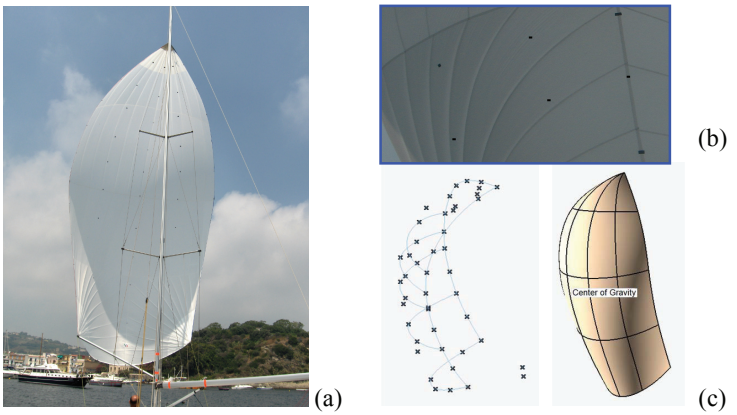

Fig. 7. (a) marker acquisition; (b) marker on the sail; (c) 3D NURBS surfaces.

4. Result

Three wind longitudinal velocities (10 m/s, 15 and 20 m/s) were taken into account to evaluate and compare the influence of sail cloth constitutive characteristics on sail dynamic performance. Rotating the sail around its vertical axis by 15°, 30° and 45° the forces, pressure distributions and vibration of/on the different sail cloths were evaluated in correspondence to 165°, 150° and 135° AWA (Fig.8a, b and c). In the simulations it was assumed that the air flow at the tunnel entrance (inlet velocity) is laminar, setting a value of maximum wind turbulence of 2%. The dynamic performances of the spinnaker obtained in correspondence of the ten different sail cloths were compared by comparing *Eddy Turbulence Kinetic Energy*. *Eddy Turbulence Kinetic Energy* are seen to be proportional to sail

edge vibrations to that acts on the sail. Fig. 8d shows the maximum sail edge displacement in correspondence to 20 m/s and 135° *AWA*. Furthermore, using the inverse formula of wind action shape (or aerodynamic) coefficient c_p was calculated with the following equation:

$$c_p = \frac{2p}{\rho \cdot V^2} \tag{2}$$

where ρ is air density [g/dm³], p is the pressure simulated at the sail surface and V is the logitudinal wind speed.

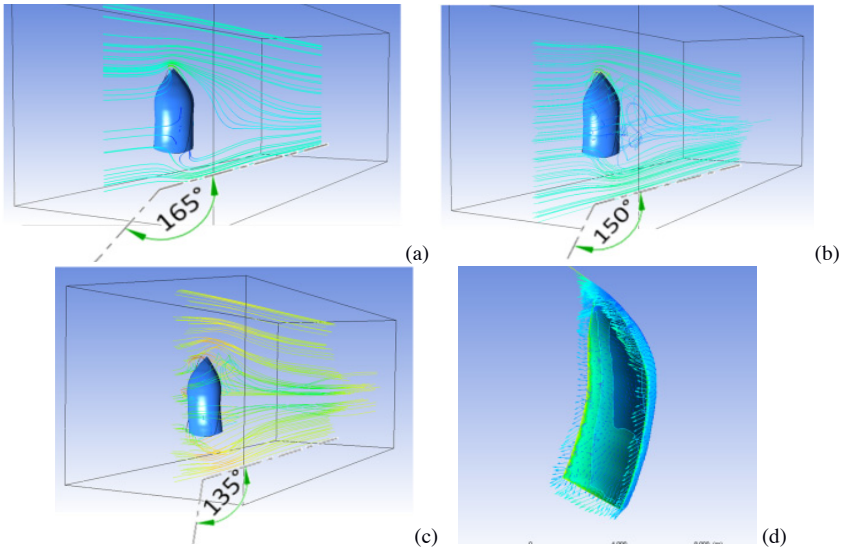

Fig. 8. Wind particle track in virtual tunnel: (a) AWA 165°; (b) AWA 150°; (c) AWA 135°; (d) maximum displacement in sail edge.

This coefficient gives an equivalent measure of the sail cloth's influence on the dynamic sail performance. The results are summarized in Table 4 below. The three values of c_p were calculated in correspondence to the three *AWA* (165°, 150° and 135°) and *Eddy Turbulence Kinetic Energy* in 1 second for a wind velocity of 20 m/s. Analyzing *SS* values shown in Tab.2, turbulence kinetic energy dissipation and the aerodynamic coefficient c_p the following conclusions can be drawn. Dacron© showed the best performance. If compared to the other samples, the Nylon cloth appeared to be more flexible, thus showing a highly wind-sensitive behaviour. For this reason it should be more suitable in light-wind and trade wind conditions. The cloths 2, 3 and 4 with full-radial panel provide the best combination in terms of stiffness in weft, warp and bias orientations, indicating minimal variations in shape during the changes in wind direction.

Table 4. Turbulence kinetic energy dissipation and shape coefficient.

Sample N°	*Cloth*	*Turb. Kinetic Energy*[kJ]			c_p		
		165°	*150°*	*135°*	*165°*	*150°*	*135°*
1	Custom Carbon	49.1	59.1	78,4	2.22	2.13	2.08
2	Nylon SPI	86.9	104.4	139,2	1.98	1.85	1.83
3	Kevlar FLEX	58.3	69.6	92,8	2.20	2.13	2.08
4	Hydranet	73.5	88.6	118,4	2.12	2.04	2.00
5	DIAX 60P	63.7	75.1	100,8	2.18	2.10	2.04
6	Kevlar CZ 15	82.6	98.0	131,2	2.02	1.94	1.89
7	Pentex FLEX 13	56.2	67.1	89,6	2.20	2.14	2.10
8	PX 15T	59.8	72.8	96	2.19	2.11	2.07
9	Pentex FLEX 15	52.7	62.3	83,2	2.21	2.13	2.08
10	Dacron© TNF 240	45.4	54.0	72	2.26	2.18	2.13

5. Conclusions

The present paper described a methodology for the implementation of anisotropic behaviour of woven and laminated fabrics in the field of sail dynamic simulations with turbulence.The constitutive relations of ten prevailing sail cloths were measured experimentally, implemented into aerodynamic simulations and their influence on sail performance was compared. Using photogrammetry, a detailed 3D reconstruction of sail flying shapes was undertaken and used to validate aerodynamic model. In particular, the present research was devoted to the study of the impact that the different distribution of fibres has on sail performance in terms of aerodynamic coefficient. This methodology can bridge the gap between the aerodynamic simulation and the real dynamic performance of sails via anisotropic material characterization. The numerical data acquired from the sail aerodynamic simulation will ensure an effective comparison between the performance of different sail cloths and provide useful data to the sail makers early in the design phase.

Acknowledgements

The authors wish to acknowledge the invaluable support of Banks Sails Membrane Naples.

References

[1] Deparday, J., Bot, P., Hauville, F., Augier, B., Rabaud, M., Motta, D., Le Pelley, D., 2016. Modal analysis of pressures on a Full-Scale Spinnaker. In: Proceedings of the 22nd Chesapeake Sailing Yacht Symposium. Annapolis, pp. 98–110.

[2] Deparday, J., Bot, P., Hauville, F., Motta, D., Le Pelley, D.J., Flay, R. G., 2014. Dynamic measurements of pressures, sail shape and forces on a full-scale spinnaker. In: Proceedings of the 23rd HISWA Symposium on Yacht Design and Yacht Construction. Amsterdam, pp. 61–73.

[3] Augier, B., Bot, P., Hauville, F., Durand, M., 2012. Experimental validation of unsteady models for fluid structure interaction: application to yacht sails and rigs. J. Wind Eng. Ind. Aerodyn. 101, pp.53–66.

[4] Black, J.T., Pitcher, N.a., Reeder, M.F., Maple, R.C., 2010. Videogrammetry dynamics measurements of a lightweight flexible wing in a wind tunnel. J. Aircr. 47 (1), pp.172–180.

[5] Viola, I.M., Bartesaghi, S., VanRenterghem, T., Ponzini, R., 2014. Detached Eddy Simulation of a sailing yacht. Ocean Eng., 90, pp. 93-103.

[6] Viola, I.M., Biancolini, M. E., Sacher, M., & Cella, U., 2015. A CFD-based wing sail optimisation method coupled to a VPP. In 5th High Performance Yacht Design Conference, pp. 1–7.

[7] Calì, M., Speranza, D., and Martorelli, M., 2017. Dynamic spinnaker performance through digital photogrammetry, numerical analysis and experimental tests. In Advances on Mechanics, Design Engineering and Manufacturing. Springer International Publishing, pp. 585–595.

[8] Martorelli, M., Pensa, C., Speranza, D., 2014. Digital Photogrammetry for Documentation of Maritime Heritage. Journal of Maritime Archaeology, 9(1), pp. 81–93.

[9] Moos, S., Marcolin, F., Tornincasa, S.,Speranza, D., Padula, F., et al. Cleft lip pathology diagnosis and foetal landmark extraction via 3D geometrical analysis, International Journal on Interactive Design and Manufacturing, Springer, pp. 15, 2014, ISSN: 1955-2513, DOI: 10.1007/s12008-014-0244-1.

[10] Vezzetti, E., Speranza, D., et Al., Exploiting 3D Ultrasound for Fetal Diagnostic Purpose through Facial Landmarking. Image Analysis & Stereology, International Society for Stereology (ISS), ISSN 1580-3139, pp. 1-22, doi: 10.5566/ias.1100, 2014;33.

[11] Gerbino S., Del Giudice D.M., Staiano G., Lanzotti A., Martorelli M. (2016), On the influence of scanning factors on the laser scanner-based 3D inspection process, INTERNATIONAL JOURNAL ADVANCED MANUFACTURING TECHNOLOGY, Vol. 84, p. 1787-1799, ISSN: 0268-3768, doi: 10.1007/s00170-015-7830-7.

[12] Logozzo, S., Zanetti, E. M., Franceschini, G., Kilpelä, A., & Mäkynen, A., 2014. Recent advances in dental optics–Part I: 3D intraoral scanners for restorative dentistry. Optics and Lasers in Engineering, 54, pp.203-221.

[13] Calì, M., & Savio, F. L., 2017. Accurate 3D reconstruction of a rubber membrane inflated during a Bulge Test to evaluate anisotropy. In Advances on Mechanics, Design Engineering and Manufacturing. Springer International Publishing, pp. 1221-1231.

[14] Calì, M., Oliveri, S. M., Fatuzzo, G., & Sequenzia, G., 2017. Error control in UAV image acquisitions for 3D reconstruction of extensive architectures. In Advances on Mechanics, Design Engineering and Manufacturing. Springer International Publishing, pp. 1209-1219.

[15] Martorelli M., Lepore A., Lanzotti A. (2016), Quality Analysis of 3D Reconstruction in Underwater Photogrammetry by Bootstrapping Design of Experiments, International Journal of Mechanics, ISSN: 1998-4448, Vol. 10, pp.39-45.

[16] E.M. Zanetti, M. Perrini, C. Bignardi, A.L. Audenino, “Bladder tissue passive response to monotonic and cyclic loading”, J Biorheology Vol. 49(1), IOS Press, 2012: 49-63. ISSN: 0006-355X.

[17] Baronio, G., Harran, S., & Signoroni, A., 2016. A Critical Analysis of a Hand Orthosis Reverse Engineering and 3D Printing Process. Applied Bionics and Biomechanics.